NJC

PAPER

View Article Online
View Journal

Cite this: DOI: 10.1039/c6nj02956f

Extended cavity pyrene-based iptycenes for the turn-off fluorescence detection of RDX and common nitroaromatic explosives†‡

Albert F. Khasanov,[a] Dmitry S. Kopchuk,[ab] Igor S. Kovalev,[a] Olga S. Taniya,[a] Kousik Giri,[c] Pavel A. Slepukhin,[ab] Sougata Santra,*[a] Matiur Rahman,[a] Adinath Majee,[d] Valery N. Charushin[ab] and Oleg N. Chupakhin[ab]

Received 19th September 2016,
Accepted 24th January 2017

DOI: 10.1039/c6nj02956f

rsc.li/njc

Extended cavity pyrene-based iptycenes have been synthesized by using the Diels–Alder reaction between *in situ* generated dehydropyrenes and anthracene. The photophysical properties and the interaction of these iptycenes with nitro-explosive components were studied both in solution and in the solid state by using fluorescence spectroscopy and X-ray crystallography, respectively. Due to the presence of both the large iptycene cavity and the central pyrene core, an unprecedently high fluorescence-quenching response towards non-aromatic and non-planar 1,3,5-trinitroperhydro-1,3,5-triazine (RDX) has been observed both in solution (with an apparent Stern–Volmer constant value $^{a}K_{SV}$ up to 1.53×10^{3} M^{-1}) and in the vapor phase (50–75% fluorescence quenching of the PU films doped with chemosensors). In the case of nitroaromatic explosives, nitrobenzene (NB), 2,4-DNT, TNT, and 2,4,6-trinitrophenol (TNP or picric acid, PA), pyrene-based iptycenes also demonstrate a good fluorescence-quenching response both in solutions (with apparent Stern–Volmer constant values $^{a}K_{SV}$ = 0.4–8.0 $\times 10^{3}$ M^{-1}) and in the vapor phase (up to 90% fluorescence quenching of the PU films doped with chemosensors). The "sphere of action" fluorescence quenching model was suggested.

Introduction

The efficient remote sensing of nitro-explosives (Fig. 1), especially the most commonly used TNT and RDX, is in high demand due to the increasing threat of terrorist attacks worldwide.[1] In addition to traditionally used canine dogs,[2] for the trace detection of nitro-explosives as well as their post-blast products, various analytical methods have been employed like separation and/or detection methods such as capillary[3] or nano-capillary electrophoresis,[4] ion mobility spectrometry (IMS),[5] ion chromatography (IC),[6] high performance liquid chromatography (HPLC),[7] as well as mass-spectrometry[8] and optical spectroscopic methods.[9] These methods are highly efficient for both civilian and military applications; however, high cost and lack of portability are the major disadvantages of these techniques.

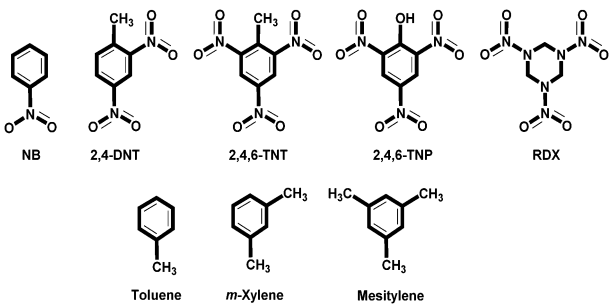

Fig. 1 The most common nitro-explosives and their possible aromatic model compounds.

Some other methods are based on colorimetric detection, detection by means of molecularly imprinted photonic crystals,[10] polymers,[11] or materials,[12] as well as fluorescence-based methods.[13–16] Various types of chemosensors/sensory materials have been reported, which are fluorescent polymeric materials,

[a] Department of Organic and Biomolecular Chemistry, Chemical Engineering Institute, Ural Federal University, 19 Mira Str., Yekaterinburg, K-2, 620002, Russian Federation. E-mail: sougatasantra85@gmail.com, ssantra@urfu.ru
[b] I. Ya. Postovskiy Institute of Organic Synthesis, Ural Division of the Russian Academy of Sciences, 22 S. Kovalevskoy Str., Yekaterinburg, 620219, Russian Federation
[c] Centre for Computational Sciences, School of Basic and Applied Sciences, Central University of Punjab, City Campus, Mansa Road, Bathinda-151001, India
[d] Department of Chemistry, Visva-Bharati (A Central University), Santiniketan-731235, India

† Dedicated to Professor Vladimir L. Rusinov on the occasion of his 70th Birthday.

‡ Electronic supplementary information (ESI) available: Synthetic procedures and spectral characterization data (^{1}H, ^{13}C NMR, and ESI mass spectra) for compounds **2–4**, binding studies, theoretical calculations, and X-ray structural data. CCDC 1486665 (**3**·nitrobenzene) and 1485942 (**3**·mesytilene). For ESI and crystallographic data in CIF or other electronic format see DOI: 10.1039/c6nj02956f

such as supramolecular[17a,b] or covalently-bonded[17c–j] polymers; dendrimers;[18] single molecule chemosensors like phosphole oxides,[19a] calix[4]arenes,[19b,c] electron-rich polyheteroaromatic compounds,[19d] including push–pull fluorophores,[15b,19e–g] oligoarenes[19h] or hetarenes;[19i–k] and organo-inorganic composites[19l–n] and metal–organic frameworks.[20] Pyrene derivatives are commonly used as fluorophores in all types of such sensor materials[21a–e] or single molecule chemosensors[19b,21f–m] for the visual detection of nitro-explosives in the vapor phase,[21b,d] or in solutions,[21] including aqueous media.[21h,g,k–m,22]

On the other hand, since the pioneering discovery of Swager and Yang,[23] 1,4-disubstituted [1.1.1*b*.1.1]pentiptycenes have become the most popular building blocks for designing highly efficient materials for the detection of NACs,[14b,24] as well as other applications.[24,25] Very recently it was confirmed by the theoretical calculations of Enrow[26] and by the experimental data of Anzenbacher Jr. and co-workers[27] that the molecular cavity of 1,4-disubstituted pentiptycenes[28] can reversibly accommodate molecules of NACs to form stable donor–acceptor complexes.

It is worth mentioning that most of the reported chemosensors/sensory materials for the turn-off fluorescence detection of nitroaromatic explosives, demonstrated either weak[17h,19a,21h,27,29a,b] or no response[21i,29c] towards non-aromatic nitro-explosives, including RDX. For instance, fluorescence quenching based sensors for the detection/identification of RDX have been reported by a few research groups, for example, phosphole oxide reported by Tanaka,[19a] supramolecular cross-reactive arrays reported by Anslyn,[21h,29a] tris(phenylene)vinylene polymer reported by Dichtel,[29b] polysilafluorenes reported by Trogler,[29c] or NAD^+/NADH-sensitive modified CdSe/ZnS quantum dots reported by Freeman and Willmer.[29d] Additionally, Zang and co-authors demonstrated a fluorescence quenching based-probe for the detection of UV-photolysis products of RDX, HMX (or PETN).[29e] Turn-on detection approaches are very limited; one is Swager's report on hydroacridinium-based dye[29f] and another is a very recent report by Anzenbacher Jr. and co-authors[29g] on a pyrene-based probe for the turn-on detection of RDX as well as for the turn-off detection of nitroaromates. Thus, investigation towards new systems for the detection of non-aromatic nitro-explosives is necessary and in demand.

Very recently, we have reported water-soluble pyrene derivatives for the fluorescent detection of nitro-explosive components as well as some herbicides in aqueous media.[21l] Inspired by recent publications of Anzenbacher Jr. and co-workers[27,28,29g] in this present manuscript we wish to report an efficient synthetic design of new extended cavity pyrene-based iptycenes for the turn-off fluorescence detection of nitro-explosives in organic solutions and in the vapor phase. The high selectivity and sensitivity of these iptycenes have been confirmed by their enhanced fluorescence quenching in the presence of trace amounts of RDX as well as nitroaromatics.

Results and discussion

Synthesis

Construction of pyrene-based iptycenes has been carried out by two aryne-based approaches. The first approach is the reaction

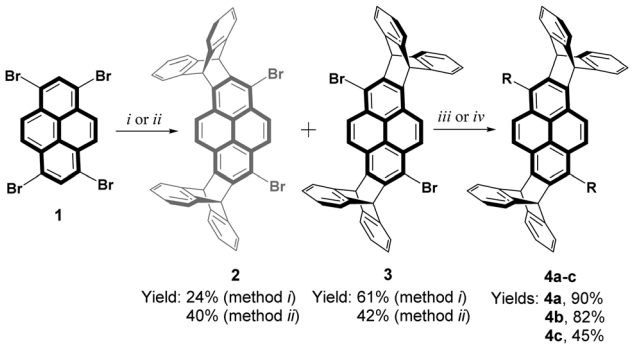

Scheme 1 Synthetic route for iptycenes **2**, **3**, and **4a–c**. *Reagents and conditions*: (i) $NaNH_2$/*t*-BuONa, anthracene, xylenes, 140 °C, 48 h; (ii) *t*-BuOK, anthracene, melt, 210 °C, 22 h; (iii) *n*-BuLi, THF, −78 °C, 1 h, then MeOH or H_2O, −78 to 25 °C, overnight; (iv) R-$SnBu_3$, toluene, PPh_3/$PdCl_2(PPh_3)_2$, reflux, 24 h.

of 1,3,6,8-tetrabromopyrene[30] **1** with $NaNH_2$/*t*-BuONa and a 10-fold excess of anthracene in dry xylene (path i). In the second approach, interaction of **1** with *t*-BuOK and anthracene in melt (path ii) afforded a mixture of iptycenes **2** and **3** in up to 85% total yield (Scheme 1 and Tables 1–2). The less-soluble isomer **3** can be easily isolated as a 1 : 1 complex with toluene by stepwise crystallization from toluene. The molecular structures of the desired compounds **2–3** were confirmed by using ^1H and ^{13}C NMR, and EI-MS.

X-Ray studies

For a more conclusive remark, the single crystal X-ray crystallography analysis of compound **3** has been performed to provide the most direct description of the molecular packing features. At first, aiming to examine the host–guest interactions in the solid state, several experiments for the co-crystallization of iptycenes **3–4** with various nitroaromates were performed. We observed some co-crystallization between NACs and compounds **3–4;** however in most cases either appropriate crystals could not be obtained or the obtained crystals could not be resolved. Only the co-crystallization of **3** from toluene (used as a competitive solvent)-nitrobenzene solution afforded good quality crystals of the stable 2 : 1 double-decker-like "iptycene **3***$PhNO_2$" inclusion complex.[31] According to X-ray data, the compound is crystallized in a centrosymmetric space group as a solvate. The geometry of the iptycene molecule is similar to that reported previously for iptycenes.[25f,27,28] In particular, the aromatic moieties are located at an angle close to 120° relative to the plane of the pyrene core. Two iptycene molecules form dimers *via* π–π-stacking with a distance of ~3.5 Å between the centroids of the molecules (Fig. 2, top). The nitrobenzene molecule is located in the molecular cavity of one iptycene molecule virtually coplanar to the plane of the pyrene core (the dihedral angle between the plane of nitrobenzene and the pyrene fragment is 10.8°). The minimal intercentroid distance from the centroid of the nitrobenzene molecule to the plane pyrene core is close to 3.6 Å, and the minimum distance from the plane of carbon atoms to the pyrene moiety is around 3.3 Å, which allows effective π–π-interaction between iptycene and nitrobenzene molecules (Fig. S89 and S90, ESI‡).

Table 1 Scope and limitations

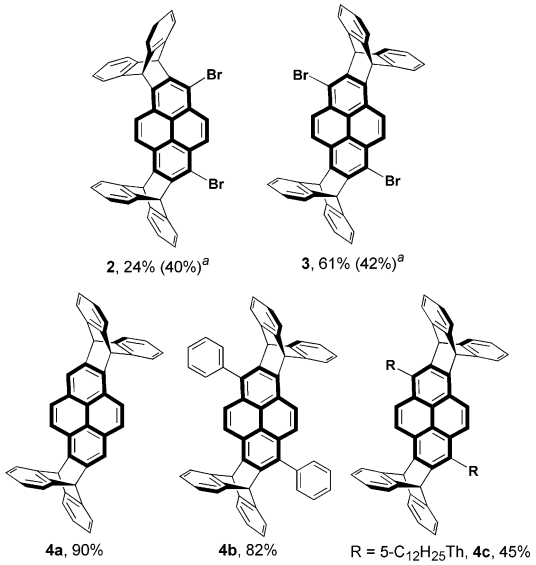

[a] For method ii.

Table 2 Photophysical properties and quenching constants for iptycenes **2–4**

#	λ_{abs} nm	λ_{em} nm	Φ_F[a]	K_{SV}^{DNT} M^{-1}	K_{SV}^{TNT} M^{-1}	K_{SV}^{TNP} M^{-1}
2	304, 356, 373	399 420	0.10	374	398	—
3	337, 346, 358, 378	399 420 440	0.05	374	384	8237
4a	343, 360, 369, 389	390 399 411	0.64	836	1321	8354
4b	342, 358, 376, 395	399 420 453	0.41	1132 959[b]	1194 1054[b]	7924 —
4c	369, 379, 398	404 426	0.18	665	1013	6896

[a] Absolute quantum yield. [b] In toluene solution.

The remaining nitrobenzene molecules are located in cavities between the iptycene dimers and no other closer intermolecular contacts were observed.

The molecule of nitrobenzene fits into the cavity formed by the iptycene receptor **3** in a face-to-face mode, and the resulting iptycene-nitrobenzene co-crystal shows nearly parallel molecular stacks. In addition, within the crystal, the iptycene molecules are arranged in ribbon-like architectures due to strong π–π-interactions between electron-rich aromatic walls of iptycene molecules with a minimum interplanar distance of ~3.4 Å. These π–π-interactions help to stabilize the neighboring stacks, and on the other hand it has been proposed and demonstrated[21d] that π–π stacking is highly favorable for exciton transportation *via* co-facial intermolecular electronic coupling due to the so-called "molecular wire" amplification.[24a,32]

Crystallization of iptycene **3** from more bulky mesitylene afforded the "iptycene **3***mesitylene" inclusion complex in a 1 : 1 ratio. The mesitylene molecule shows some similarity to

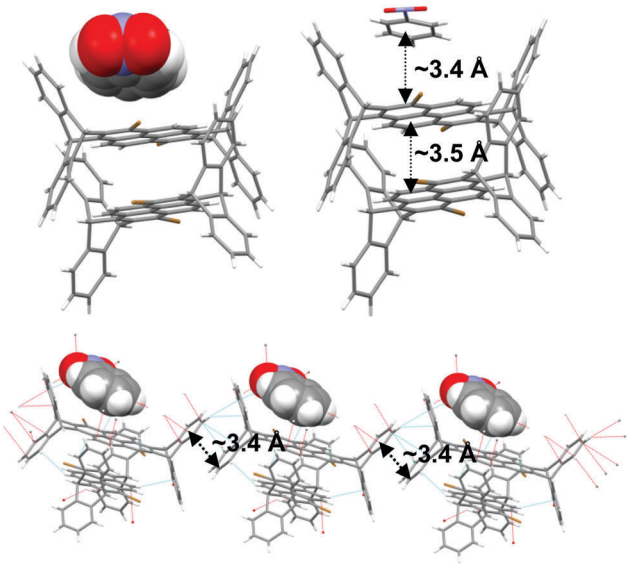

Fig. 2 Top: Molecular structure of the "iptycene **3** nitrobenzene" complex structure (single crystal X-ray diffraction, CCDC 1486665). The interplanar distances between two pyrene moieties of the iptycene and the pyrene moiety and a nitrobenzene molecule are indicated. Bottom: The crystal packing of compound **3**. The interplanar distances between the phenylene moieties of the iptycene are indicated.

both 1,3,5-trinitrobenzene, TNT and RDX (Fig. 1), so we assume it can be used as a model compound to simulate the possible binding mode between iptycenes **3–4** and nitro-explosives. According to the X-ray analysis data (Fig. 3),[33] like nitrobenzene, the bulky mesitylene molecule fits into the cavity formed by the iptycene receptor **3** in a face-to-face mode with almost parallel arrangement of both molecular planes with a minimum distance of ~3.4 Å. The molecules are placed in the centrosymmetric packing of the triclinic system. However, the solution in the $P\bar{1}$ space group led to disordering of the solvate by generating inadequate bond distances and contacts and a reasonable structural model can be formed only in the chiral space group *P*1. The plane of the benzene ring of the solvate is oriented at the angle of 6.4° towards the plane of the pyrene moiety and the distance from the centroid of the benzene ring to the plane of the pyrene moiety is approximately 3.55 Å. Shortened interatomic contact is observed for the Me-group of the solvate with the C9S···C24 distance of 3.38 Å. (Fig. S91 and S92, ESI‡).

These results suggest that due to the larger cavity the pyrene-based iptycenes are able to bind with both nitroaromatic and

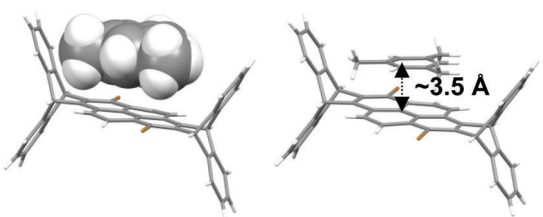

Fig. 3 Molecular structure of compound **3** with a mesitylene structure (single crystal X-ray diffraction, CCDC 1485942). The interplanar distances between the pyrene moiety and the mesitylene molecule are indicated.

bulky aromatic compounds, in a face-to-face fashion in the solid state. It is worth mentioning that the X-ray results for pyrene-based iptycenes differ from the earlier reported results for pentiptycenes by Anzenbacher Jr.,[27] where the nitrobenzene molecule enters into the iptycene cavity almost perpendicular to the central benzene ring and displays an edge-to-face binding mode. Our present system is more favorable, as we assume that the binding mode can be explained by the larger cavity of iptycenes **3–4** due to the presence of an electron-rich pyrene moiety in the central core of the receptor.

Pyrenes themselves are known to form stable molecular complexes with both aromatic[34a] and nitro-aromatic[34b–d] compounds in a face-to-face mode *via* π–π-stacking. Therefore, stronger interactions are expected in the case of more electron-deficient poly-nitrated aromatic compounds, such as 2,4-DNT, TNT and others. In addition, extra bonding between NACs and the electron-rich walls of the iptycene receptor is also expected.

Fluorescence quenching studies

The photophysical properties of iptycenes **2–4** were investigated by using UV/Vis and fluorescence spectroscopy. Thus, the absorption spectra of chromophores **2–3** exhibit two major bands centered at *ca.* 290–310 nm and 340–360 nm attributed to the electronic transitions between the S_0–S_3 and S_0–S_2 energy levels along with some other vibrational bands of each transition[35] (Fig. 4). The emission spectra of iptycenes **2–3** are typical for the monomeric form of pyrene with the emission maxima centred at *ca.* 380 nm (Fig. 4, Table 1 and Fig. S2, S3, S8, S9, ESI‡).

The fluorescence quantum yields for dibromoiptycenes **2–3** are lower than that of pyrene (Table 2) which may be attributed to the fluorescence quenching by the internal heavy atom effect that encourages intersystem crossing to non-radiative triplet states.[36] As a result, we did not observe a strong fluorescence response of compounds **2–3** towards 2,4-DNT and TNT both in solution and in the solid state (Table 2 and Fig. S4–S7, S10–S18, ESI‡). The high value of the quenching constants in the case of TNP can be attributed to the suppression of the fluorescence of the pyrene moiety due to FRET since the emission spectra of receptors **2–3** overlap to a large extent with the absorption spectra of TNP.

To improve the conjugation of the fluorophores and/or the electron-donating properties in the next step, we have synthesized iptycenes **4b–c** by means of Stille cross-coupling between dibromoiptycene **3** and (hetero)aromatic organostannanes (Scheme 1 and Tables 1, 2). Whereas iptycene **4a** has been synthesized indirectly as a side-product in Stille cross-coupling (path iv) or directly by the reaction of **3** with *n*-butyl lithium (path iii) with the following quenching of *in situ* generated lithium salt with methanol or water.

As expected, compared to iptycenes **2–3** both the photophysical properties and the sensory response towards NACs improved for chemosensors **4a–c**. Thus, the fluorescence quantum yields (Φ_F) for **4a–c** increased up to 0.64 (Table 2), and *ca.* 10–30 nm bathochromic shifts were observed in both the absorption and emission maxima. In the case of sensor **4c**, the lower quantum yield value can be *vide supra*, due to the presence of two heavy (sulfur) atoms.

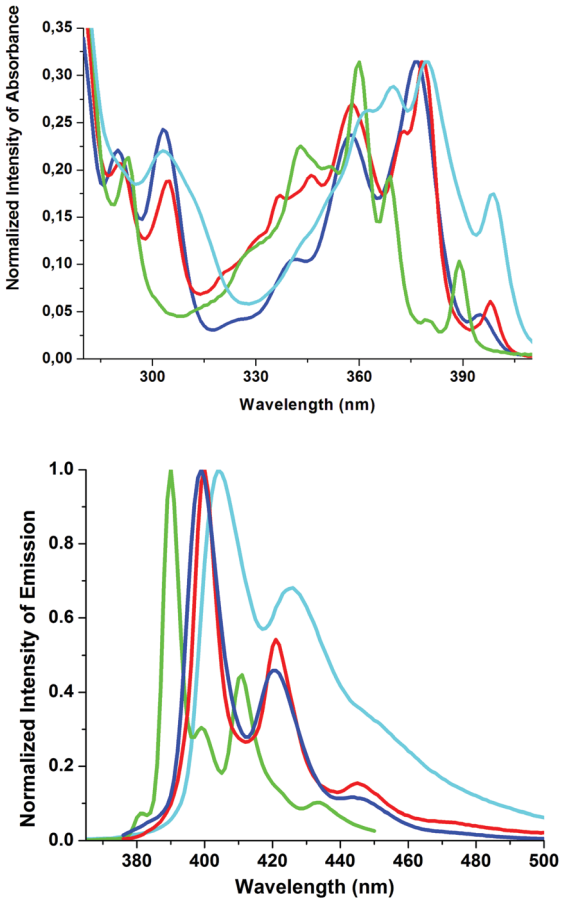

Fig. 4 Normalized absorption (top) and emission (bottom) spectra of iptycenes **3** (red), **4a** (green), **4b** (blue) and **4c** (sky blue).

Compounds **4a–c** in THF solutions exhibited a strong fluorescence response to 2,4-DNT, TNT and TNP, as was anticipated. Fig. 5 shows the result of the spectrofluorimetric titration of the most representative sensor **4a** (1.00×10^{-6} M) with incremental concentrations of TNT upon excitation with UV-light (λ_{ex} = 375 nm). By increasing the concentration of TNT, the fluorescence intensity of **4a** gradually depletes, showing up to 90% quenching (Fig. 5a and Fig. S24, ESI‡). The Stern–Volmer plot shows that the quenching process is nonlinear with the increased concentration of the quencher (TNT) (Fig. S25, ESI‡). These observations support the commonly accepted mechanism of quenching as a result of static quenching at the low concentration of the quencher and the combined dynamic and static quenching at higher concentration. Based on the time-resolved fluorescence emission of compound **4a,** the possible role of collisional or dynamic quenching at low concentration of the quencher was ruled out as the decay lifetime of *ca.* 4.78 ns of chemosensor **4a** was constant, being independent of the TNT concentration (Fig. 5b and Fig. S60–S68, Table S1, ESI‡).

The data obtained from the SV plots indicate high values of the apparent Stern–Volmer constants in the case of TNT ($^aK_{SV}^{TNT}$ = 1.0–1.3 × 10^3 M^{-1}), TNP ($^aK_{SV}^{TNP}$ = 6.9–8.3 × 10^3 M^{-1}) and 2,4-DNT ($^aK_{SV}^{TNT}$ = 0.7–1.1 × 10^3 M^{-1}) (Table 2, Fig. 5a and

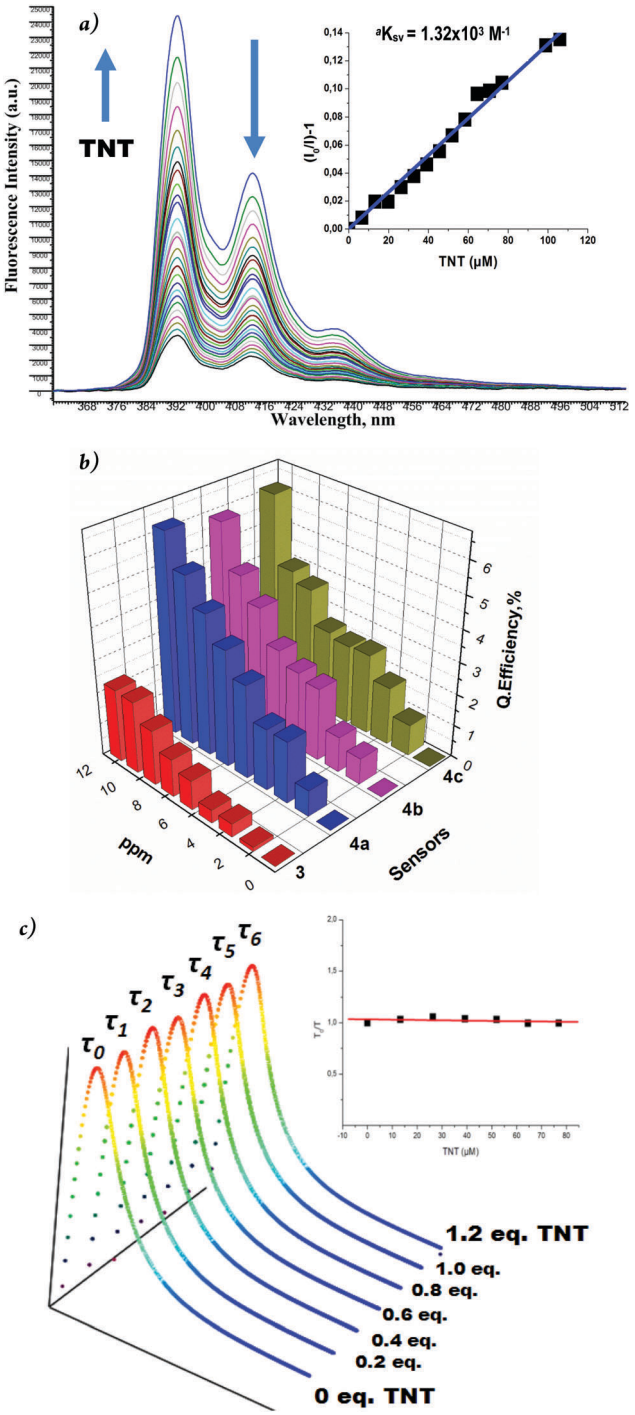

Fig. 5 (a) Fluorescence quenching of sensor **4a** in the presence of TNT. The inset shows the Stern–Volmer plot; (b) TNT detection limit graphs for sensors **3–4**; (c) fluorescence decay profiles for sensor **4a** in the presence of TNT. The inset shows the τ_0/τ_{1-6} ratios. The excitation wavelength was 375 nm and the solvent was THF.

Fig. S21–S57, ESI‡) calculated for chemosensors **3–4**, the detection limit for TNT is lower than 1 ppm (Fig. 5b). Even in toluene solution (as a competitive solvent) the apparent Stern–Volmer constant values were relatively high (Table 2, compound **4b**) and comparable with the constants observed for the iptycene-based amplifying polymers[23] (K_{SV} = 1.17 × 10^3 M^{-1})[17f] or polysilole sensors (K_{SV} = 4.34 × 10^3 M^{-1}),[17f] and they were higher than that of pyrene itself (K_{SV} = 3.1–3.9 × 10^2 M^{-1}).[21i] As for previously reported 1,4-disubstituted [1.1.1*b*.1.1]pentiptycenes ($^{a}K_{SV}$ = 1.0–4.5 × 10^3 M^{-1})[27a] their apparent abilities for NAC detection could be affected by inner-filter effects since they were excited at the shorter wavelength (λ_{ex} = 300 nm). In order to substantially reduce the above effects, the present compounds were excited at longer wavelengths (λ_{ex} = 375 nm). The best sensory response towards nitroaromates has been observed in the case of non-substituted iptycene **4a** (Fig. S57, ESI‡), which can also be explained by the higher ability of the non-substituted iptycene cleft to fit in larger nitroaromatics. Indeed, the $^{a}K_{SV}$ values reported for 2,4-DNT and TNT are apparently higher than those reported previously.[17f,27a]

This high quenching efficiency of the emission of chemosensors **4a–c** upon the addition of NACs can be primarily attributed to the static quenching mechanism due to the possible formation of a non-fluorescent donor–acceptor complex in the ground state *via* strong π–π interactions between the nitroaromatic quencher and the pyrene moieties of **4a–c** and/or so-called "sphere-of-action" quenching. In our experiments in the UV-Vis spectra of the most representative iptycene **4a,** the pyrene moiety absorbance bands were found to be stable during the titrations by NACs (Fig. S31–S32, ESI‡), so no stable π–π-complex formation was observed. These results may indicate the so-called false static (quasistatic) quenching due to "sphere of action".[37] The commonly accepted Perrin model describes this case of (false) static quenching between randomly distributed fluorophores and quenchers that are located in proximity. In this model, one assumes that there is instantaneous quenching of an excited donor by a quencher molecule, if the quencher is located inside a sphere of volume V_q around the fluorophore and there is no quenching when the quencher is outside of this quenching sphere.[38] It is common, that in "sphere of action" fluorescence quenching no ground state complex is formed.[37]

In order to demonstrate the selectivity of iptycenes **3–4** toward nitroaromatic compounds, we carried out a fluorescence titration experiment using a non-explosive compound (such as benzoquinone (BQ)), which also displays high electron affinity. Only sensor **4a,** which shows the highest sensitivity towards NACs, exhibited a very weak fluorescence quenching response to BQ even at very high concentrations (2.0 × 10^{-2} M) with the apparent Stern–Volmer constant of $^{a}K_{SV}^{BQ}$ = 0.38 × 10^3 M^{-1} (Fig. S31 and S32, ESI‡), while the other sensors exhibited only subtle changes in the fluorescence spectra in the presence of high concentrations of BQ.

As a next step, we investigated the interaction of the best sensor **4a** with a non-aromatic nitro-explosive, *i.e.* RDX. It was reported before that both pyrene[21i] and 1,4-disubstituted [1.1.1*b*.1.1]pentiptycenes[27a] demonstrated very weak interactions with RDX at the limit of the diffusional quenching mechanism due to both steric factors and the high LUMO energy restricting the significant PET quenching. In our experiments, due to both of its pyrene-based central moiety and the larger cavity, the sensor **4a** demonstrated a very pronounced fluorescence quenching response to RDX with a Stern–Volmer constant value as high as

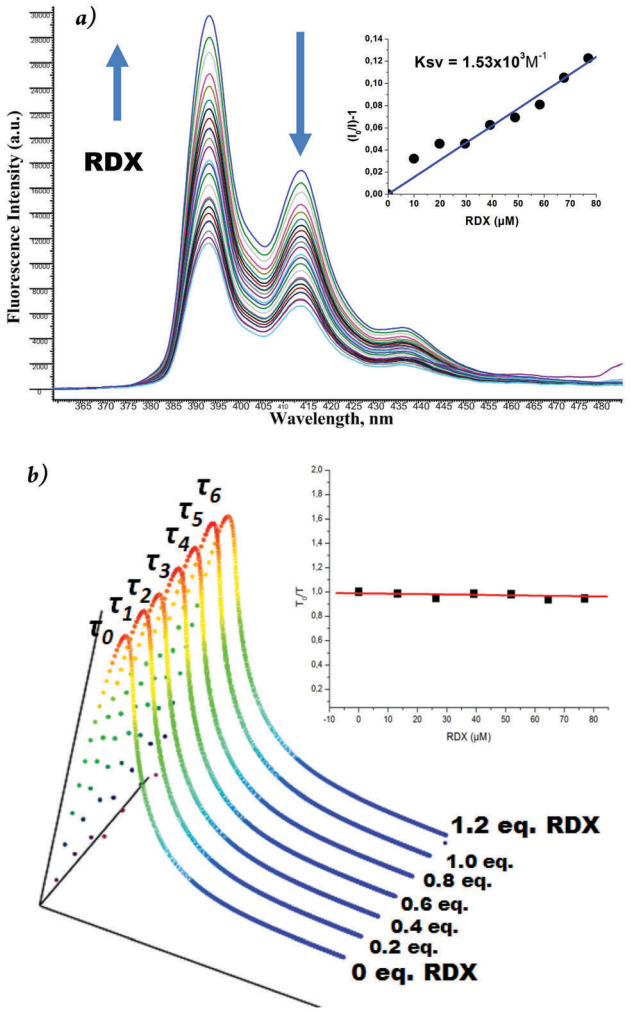

Fig. 6 (a) Fluorescence quenching of sensor **4a** in the presence of RDX. The insert shows the Stern–Volmer plot; (b) fluorescence decay profiles for sensor **4a** in the presence of RDX. The insert shows the τ_0/τ_{1-6} ratios. The excitation wavelength was 375 nm and the solvent was THF.

1.53×10^3 M^{-1}. Fig. 6 shows the result of spectrofluorimetric titration of sensor **4a** (1.00×10^{-6} M) with incremental concentrations of RDX upon excitation with UV-light (λ^{ex} = 375 nm). Likewise for NACs, upon increasing the concentration of RDX the fluorescence intensity of **4a** decreases (Fig. 6a). The Stern–Volmer plot demonstrates the close to linear fluorescence-quenching response with the increased concentration of RDX. Most probably in the case of RDX only one quenching mechanism, *i.e.* sphere of action static quenching, could possibly be the prevailing mechanism. To confirm that mechanism, the time-resolved fluorescence emission of chemosensor **4a** in the presence of RDX has been investigated (Fig. 6b and Fig. S69–S77, Table S2, ESI‡). Thus, it has been concluded that the decay lifetimes of chemosensor **4a** were constant values of 4.78 ns, being independent of the concentration of RDX. The quenching efficiency of sensor **4a** in response to RDX is better than that of 2,4-DNT and TNT (Fig. 7). It is worth mentioning that chemosensor **4a** demonstrates a higher value of the Stern–Volmer constant for RDX than pyrene itself[21i] and other chemosensors,[14e]

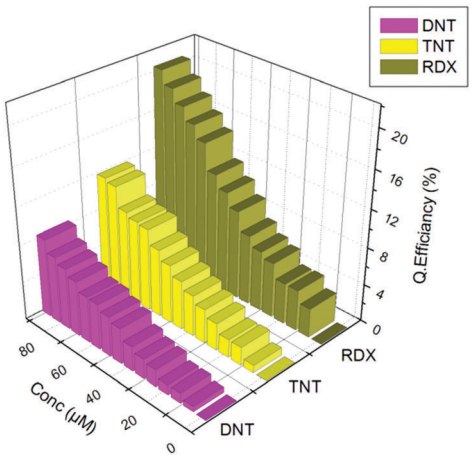

Fig. 7 Quenching efficiency of **4a** depending on the quencher type.

and also demonstrates a comparable value with a pyrene-based turn-on probe for RDX reported by Anzenbacher Jr. and co-workers.[29g]

DFT modeling and studies

In order to fully understand the nature of the interaction of RDX with sensor **4a** and to provide further support to the observed high fluorescence quenching response toward RDX, density functional theory (DFT) calculation was carried out using the Gaussian 09[39] suite of programs and employed the density functional theory method using the Austin–Frisch–Petersson functional with dispersion corrections[40] and the balanced polarized triple zeta basis set of Ahlrichs and co-workers.[41]

After each geometry optimization, frequency calculations were performed to ensure the local energy minimum structures. The optimized structure of the complex of **4a** with RDX is shown in Fig. 8. As can be seen from Fig. 8, the RDX molecule shows a strong tendency to form an inclusion complex with **4a** *via* a face-to-face binding motif. The calculated minimal intermolecular distance between the molecular plane of **4a** and that of NO_2 moieties of RDX is about 3.30 Å, which suggests the possibility of π–π interactions between them.[40]

In addition to the geometry of the complex "iptycene **4a***RDX" the HOMO–LUMO energies for compounds **4a**, **4b**, and previously reported[27a] 1,4-bis(phenylethynyl)-[1.1.1*b*.1.1]pentiptycene (compound **6**) were calculated using the same program suite (Table 3 and Fig. 9). By analyzing the results of DFT-calculations,

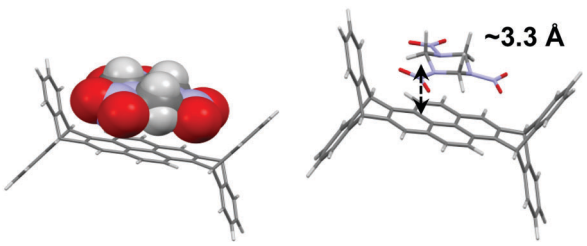

Fig. 8 Optimized structure of complex **4a**·RDX. The B3LYP/6-31G(d) level of theory was used for the calculations.

Table 3 APFD/DEF2-TZVP DFT calculations for the HOMO and LUMO of nitro-explosives and selected chemosensors

Compound	E_{HOMO}, au (eV)	E_{LUMO}, au (eV)	Compound	E_{HOMO}, au (eV)	E_{LUMO}, au (eV)
2,4-DNT	−0.31211	**−0.11373**	**3**	−0.20979	−0.07510
	(−8.4929)	**(−3.0947)**		(−5.7086)	(−2.0435)
TNT	−0.32498	**−0.13096**	**4a**	−0.20272	**−0.06276**
	(−8.8431)	**(−3.5636)**		(−5.5163)	**(−1.7077)**
PA	−0.31510	**−0.14578**	**4b**	−0.20015	−0.06287
	(−8.5743)	**(−3.9668)**		(−5.4463)	(−1.7107)
RDX	−0.32744	**−0.08901**	**6**[a]	−0.21643	−0.07338
	(−8.9101)	**(−2.4220)**		(−5.8893)	(−2.0334)
			4a-RDX	−0.20703	−0.07517
				(−5.6335)	(−2.0454)

[a] From ref. 27*a*. The best LUMO matches are indicated in bold.

one may conclude that for pyrene-based iptycenes due to their higher LUMO energies, as compared to previously reported 1,4-disubstituted pentiptycenes, PET quenching is more preferable in the presence of both aromatic (2,4-DNT, TNT and TNP) and non-aromatic nitro-explosives (RDX). The best response of compound **4a** towards RDX can be possibly explained by its highest LUMO energy of −1.70 eV, compared to compound **4b** (−1.71 eV), and compound **6** (−2.03 eV),[27a] which is 0.72 eV (69.45 kJ mol^{-1}) higher than the LUMO energy of RDX (−2.42 eV). We assume that this 0.72 eV difference is the driving force favoring the most efficient PET quenching of sensor **4a** in the presence of trace amounts of RDX.

In addition, the HOMO–LUMO band gaps for sensors **4a–b** are lower than that of for compound **6**; therefore the electronic transitions from the HOMO to the LUMO occur with lower energy (upon photoexcitation with longer wavelength UV-light). Thus, based on all of the above provided explanations one may conclude that this high affinity of sensor **4a** towards RDX is due to its larger cavity compared to previously reported iptycenes, which provides both the extra space to accommodate sterically hindered RDX molecules and some extra binding sites provided by aromatic walls of the iptycene cavity. In addition, the introduction of the pyrene moiety into the iptycene core seems to increase the LUMO energy level of pyrene-based iptycene *vs.* pentiptycenes. Therefore, the first ones have higher affinity (due to their higher LUMO) to non-aromatic nitro-explosives, such as RDX.

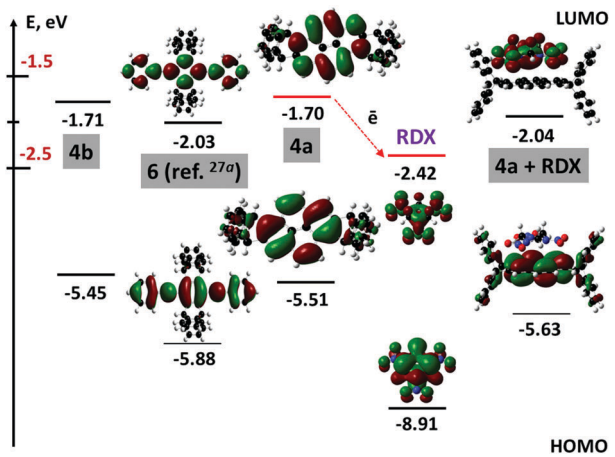

Fig. 9 DFT calculations for iptycenes **4a–b** and **6**[27a] and RDX.

Fabricating the sensor-doped polymer films and the sensory chip

As a final step in order to explore the future practical application of the herein reported chemosensors, we have prepared sensor films by doping iptycenes **3** and **4a–c** into a polyurethane matrix in order to apply the obtained polymer films for the fluorescence turn-off detection of nitro-explosives in their vapors.

For that we have solution-casted the solutions of sensors **3** and **4a–c** in polyurethane (*ca.* 5% w/w) in the wells of aluminium chips to form sensor films. After that these chips were exposed to vapors of the components of nitro-explosives (TNT, 2,4-DNT and RDX) at equilibrium. As shown in Fig. 10, depending on the nature of both the sensor and the analyte, different fluorescence quenching responses of the sensor films are observed. Thus, after 250 seconds of exposure to the TNT and 2,4-DNT vapors, observable fluorescence quenching (around 50% *vs.* unexposed films) occurred for all the sensors. After 450 seconds, around 90% fluorescence quenching occurred (Fig. 10, bottom). In the case of RDX, exposure for 450 seconds resulted in 50–75% quenching. This can be explained by the higher vapor pressures of 2,4-DNT and TNT compared to RDX. Upon re-equilibration in pure air or by washing with methanol, the fluorescence of the sensor films was recovered.

Conclusions

In summary, we have synthesized extended cavity pyrene-based iptycenes for the turn-off fluorescence detection of RDX and common nitro-aromatic explosives. Due to the presence of both the large iptycene cavity and the central pyrene core these chemosensors demonstrate high selectivity towards RDX (in the case of the most representative chemosensor **4a,** the Stern–Volmer constant value was as high as 1.53×10^3 M^{-1}) and common nitroaromatic explosives (the Stern–Volmer constant values were $^{a}K_{SV} = 0.4–8.0 \times 10^3$ M^{-1}). The "face-to-face" binding mode between sensors **2–4** and nitro-explosives was proposed to be the most probable based on both DFT calculations and single crystal X-ray diffraction studies. The "sphere of action" fluorescence quenching model was suggested based on the results

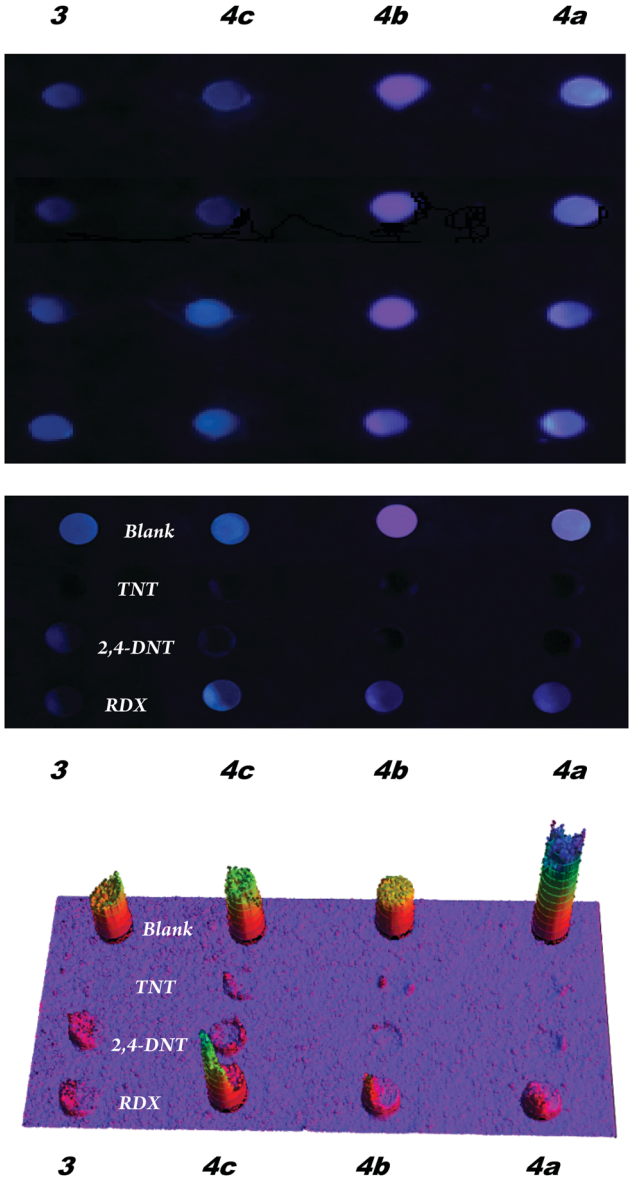

Fig. 10 Fluorescence quenching of PU films of sensors **3** and **4a–c** in air before (top) and after (middle) exposure to vapors of nitro-explosives. The 3D diagram (bottom) demonstrates the degree of quenching of the nitro-explosive-exposed films *vs.* blank.

of UV-titrations and time-resolved fluorescence emission experiments. Further practical application of chemosensors **3** and **4** has been explored by preparing sensing chips for the visual detection of NACs and RDX in the vapor phase. Thus, these present pyrene-based iptycenes **4a–c** can be used as new, easily-prepared yet sensitive chemosensors for the visual detection of nitro-explosives, especially RDX.

Experimental section

Measurements and characterization

^{1}H (400 MHz) and ^{13}C NMR (100 MHz) spectra were measured on a Bruker Avance-400 spectrometer. Fluorescence spectra were measured on Horiba-Fluoromax-4 and Ocean Optics USB4000-FL spectrofluorometers. Fluorescence titration experiments were carried out by using the Horiba-Fluoromax-4 and Ocean Optics USB4000-FL spectrofluorometers. UV/Vis absorption spectra were recorded on a Shimadzu UV-2550 spectrometer.

Materials and reagents

All chemicals and reagents were used as received from commercial sources without further purification. Solvents for chemical synthesis were purified or freshly distilled prior to use, according to standard procedures. All chemical reactions were carried out under an inert atmosphere. The synthesis of 1,3,6,8-tetrabromopyrene **1** has been described previously.[30] Compounds **4b–c** were synthesized according to the previous method.[28,42]

General procedure for the synthesis of iptycenes 2–3

Method A. A mixture of 1,3,6,8-tetrabromopyrene (1 g, 1.93 mmol), anthracene (3.44 g, 19.31 mmol), sodium *tert*-butoxide (0.77 g, 8.0 mmol) and freshly prepared sodium amide (0.16 g, 4.1 mmol) was suspended in 60 mL of dry xylene and the mixture was stirred at 140 °C for 48 h. The resulting suspension was cooled to room temperature, washed with water (3 × 50 mL) and dried over $CaCl_2$. After filtration, the solution was evaporated under reduced pressure, and the residue was separated from the excess of anthracene by using column chromatography (eluent : hexane, then dichloromethane-hexane (1 : 1)). The fractions with the same R_f were collected and evaporated under reduced pressure. After that the residue was dissolved in toluene (20 mL); the mixture was kept at −18 °C for 24 h. The resulting precipitate was filtered off to afford compound **3** as a 1 : 1 solvate with toluene (200 mg, 0.25 mmol, 13%). The rest of the solvent was evaporated under reduced pressure. The residue was separated again by column chromatography using a 1 : 1 mixture of petroleum ether and toluene as the eluent to afford the additional amount of compound **3** and compound **2**.

Method B. A mixture of 1,3,6,8-tetrabromopyrene (1 g, 1.93 mmol), anthracene (3.44 g, 19.31 mmol) and potassium *tert*-butoxide (0.65 g, 5.79 mmol) was heated at 210 °C for 22 h. The resulting melt was crushed, suspended in toluene (50 mL), washed with water (3 × 50 mL) and dried over $CaCl_2$. After filtration, the solution was evaporated to dryness and separated by column chromatography using a 1 : 1 mixture of petroleum ether and toluene as the eluent.

Compound 2. Yield 24% (Method A), 40% (Method B). M.p. > 250 °C. ^{1}H NMR ($CDCl_3$): 6.45 (s, 2H, H–C(sp^3)), 6.47 (s, 2H, H–C(sp^3)), 7.02 (m, 8H, anthracene), 7.56 (m, 8H, anthracene), 8.43 (s, 2H, pyrene), 8.58 (s, 2H, pyrene). ^{13}C NMR (DMSO-d_6): 48.6 (C(sp^3)), 53.8 (C(sp^3)), 117.0, 124.2, 124.3, 125.3, 125.4, 125.6, 125.8, 128.2, 128.9, 137.3, 143.0, 144.8, 144.8, 145.1. EI-MS (*m*/*z*): 712 (100). Anal. calcd for $C_{44}H_{24}Br_2$: C, 74.14; H 3.40. Found: C, 73.97; H, 3.32%.

Compound 3. Yield 61% (Method A), 42% (Method B). M.p. > 250 °C. ^{1}H NMR ($CDCl_3$): 6.43 (s, 2H, H–C(sp^3)), 6.48 (s, 2H, H–C(sp^3)), 7.04 (m, 8H, anthracene), 7.57 (m, 8H, anthracene), 8.33 (d, 2H, J = 9.6 Hz, pyrene), 8.48 (d, 2H, J = 9.6 Hz, pyrene). ^{13}C NMR (DMSO-d_6): 48.8 (C(sp^3)), 54.0 (C(sp^3)),

117.0, 124.1, 124.2, 124.5, 125.4, 125.6, 126.2, 126.3, 128.1, 128.8, 141.8, 143.3, 144.8, 145.1. EI-MS (*m*/*z*): 712 (100). Anal. Calcd for $C_{44}H_{24}Br_2$: C, 74.14; H 3.40. Found: C, 73.97; H, 3.32%.

General procedure for the synthesis of iptycenes 4

A mixture of iptycene **3** (75 mg, 0.100 mmol) and the corresponding organostannane (0.300 mmol), $PdCl_2(PPh_3)_2$ (7.4 mg, 0.010 mmol) and triphenylphosphine (5.5 mg, 0.02 mmol) was stirred in dry toluene (15 mL) for 24 h under reflux. The solvent was evaporated under reduced pressure and the oily residue was separated by column chromatography by using a mixture of petroleum ether and dichloromethane (20 : 1) as the eluent.

Typical procedure for the synthesis of compound 4a

Compound **3** (100 mg, 0.14 mmol) was dissolved in dry THF (25 mL) and cooled to −78 °C under argon (Schlenk procedure). *n*-BuLi solution in hexane (2.5 M, 0.12 mL, 0.31 mmol) was added dropwise at −78 °C and the resulting mixture was allowed to stand for 1 h while cooling was stopped and the temperature of the mixture was increased to room temperature. Methanol (15 mL) was added and the mixture was poured into water (50 mL). The product was extracted with benzene (3 × 25 mL); the extract was dried over Na_2SO_4. After filtration the solution was evaporated under reduced pressure to give the product as colorless crystals. An analytical sample was obtained by recrystallization from acetonitrile. Yield 70 mg (90%). ^{1}H NMR ($CDCl_3$): 5.78 (s, 2H, H–C(sp^3)), 6.38 (s, 2H, H–C(sp^3)), 6.99 (m, 8H, anthracene), 7.50 (m, 4H, anthracene), 7.95 (d, 2H, *J* = 9.2 Hz, pyrene), 8.12 (s, 2H, pyrene), 8.46 (d, 2H, *J* = 9.2 Hz, pyrene). ^{13}C NMR ($CDCl_3$): 49.9 (C(sp^3)), 55.0 (C(sp^3)), 120.2, 121.4, 123.1, 123.8, 123.9, 125.2, 125.3, 125.9, 127.5, 128.1, 139.0, 142.4, 145.4, 146.3. EI-MS (*m*/*z*): 554 (100). Anal. calcd for $C_{44}H_{26}$: C, 95.28; H, 4.72. Found: C, 95.33; H, 4.92%.

Compound 4b. Yield 58 mg (82%). ^{1}H NMR ($CDCl_3$): 5.61 (s, 2H, H–C(sp^3)), 6.41 (s, 2H, H–C(sp^3)), 6.96 (m, 8H, antracene), 7.23–7.29 (m, 4H, Ph), 7.47 (m, 8H, anthracene), 7.60–7.72 (m, 6H, Ph), 7.78 (d, 2H, *J* = 9.2 Hz, pyrene), 8.43 (d, 2H, *J* = 9.2 Hz, pyrene). ^{13}C NMR ($CDCl_3$): 50.0 (C(sp^3)), 52.1 (C(sp^3)), 121.4, 123.3, 123.7, 123.9, 125.2, 125.3, 125.4, 126.0, 126.8, 127.6, 128.5, 131.0, 132.9, 139.0, 139.2, 141.3, 145.6, 146.2. EI-MS (*m*/*z*): 706 (100). Anal. calcd for $C_{56}H_{34}$: C, 95.15; H, 4.85. Found: C, 95.02; H, 4.71%.

Compound 4c. Yield 50 mg (45%). ^{1}H NMR ($CDCl_3$): 0.88 (t, 6H, *J* = 7.2 Hz, CH_3), 1.17–1.49 (m, 36H, thiopene–$CH_2CH_2(CH_2)_9$), 1.90 (m, 4H, thiopene–CH_2CH_2), 3.05 (t, 4H, *J* = 7.2 Hz, thiopene–CH_2), 5.84 (s, 2H, H–C(sp^3)), 6.40 (s, 2H, H–C(sp^3)), 6.98 (m, 10H, anthracene, H-4 (thiophene)), 7.05 (d, 2H, *J* = 3.2 Hz, H-3 (thiophene)), 7.36 (m, 4H, anthracene), 7.48 (m, 4H, anthracene), 8.04 (d, 2H, *J* = 9.6 Hz, pyrene), 8.46 (d, 2H, *J* = 9.6 Hz, pyrene). ^{13}C NMR ($CDCl_3$): 27.2, 29.1, 29.3, 29.36, 29.4, 29.5, 29.7, 29.8, 30.4, 31.8, 31.9, 31.9, 49.9, 52.18, 121.6, 123.0, 123.8, 123.9, 124.1, 125.2, 125.3, 125.6, 125.9, 126.2, 128.5, 128.7, 136.5, 139.1, 143.1, 145.5, 146.07, 147.4. EI-MS (*m*/*z*): 1054 (100). Anal. calcd for $C_{76}H_{78}S_2$: C, 86.48; H, 7.45. Found: C, 86.33; H, 7.29%.

Fluorescence quenching studies in solution

Solutions of **2**, **3** and **4a–c** were prepared by dissolving the samples in freshly distilled dry THF. In a typical titration experiment, 1.0 mL of the solution of sensors (1–10 × 10^{-6} M) was placed in a standard quartz macrocell, followed by adding aliquots of *ca.* 0.1 molar equivalent of each nitro-explosive in a solution of the sensor.

The fluorescence emission spectra were measured (298 K) under λ_{ex} = 375 nm. The fluorescence quenching experiments were carried out by means of the titration of the solutions (1–10 × 10^{-6} M) of sensors.

Fluorescence quenching of sensors 3 and 4a–c in polymer matrices

The THF solutions of sensors **3** and **4a–c** in polyurethane (*ca.* 5% w/w) were solution-casted in wells of aluminium chips to form sensor films. After evaporation of the solvent overnight at room temperature the resulting chips were exposed to vapors of components of nitro-explosives (TNT, 2,4-DNT and RDX) at equilibrium. The fluorescence quenching of the chips was carried out by placing the sensor chip in a tall sealed glass chamber in which the analyte vapors had been equilibrated. The equilibrium vapor pressure for TNT at 25 °C is 9.4 ppb v/v,[43a] for 2,4-DNT it is 180 ppb v/v,[43b] and for RDX it is 0.006 ppb v/v.[43a] These analytes were delivered to the sample chip by diffusion. The blank samples were prepared by placing the scotch-tape film over the wells to prevent the penetration of the vapors of nitro-explosives.

Abbreviations

NB	Nitrobenzene
2,4-DNT	2,4-Dinitrotoluene
TNT	2,4,6-Trinitrotoluene
TNP	2,4,6-Trinitrophenol
RDX	1,3,5-Trinitroperhydro-1,3,5-triazine
BQ	Benzoquinone

Acknowledgements

This work was supported by the Russian Science Foundation (Ref. #16-43-02020), by Act 211 Government of the Russian Federation (Ref. 02.A03.21.0006), and, for A. M., by the BRNS–DAE (Ref. #37(2)/14/35/2014-BRNS/563, June 10, 2014). K. Giri is grateful to the UGC, New Delhi, India for Start-up Project Funding.

Notes and references

1 J. S. Caygill, F. Davis and S. P. Higson, *Talanta*, 2012, **88**, 14–29.
2 (*a*) N. Lorenzo, T. Wan, R. J. Harper, Y.-L. Hsu, M. Chow, S. Rose and K. G. Furton, *Anal. Bioanal. Chem.*, 2003, **376**, 1212–1224; (*b*) R. J. Harper, J. R. Almirall and K. G. Furton, *Talanta*, 2005, **67**, 313–327.
3 (*a*) J. P. Hutchinson, C. J. Evenhuis, C. Johns, A. A. Kazarian, M. C. Breadmore, M. Macka, E. F. Hilder, R. M. Guijt,

G. W. Dicinoski and P. R. Haddad, *Anal. Chem.*, 2007, **79**, 7005–7013; (*b*) J. J. Corr and J. F. Anacleto, *Anal. Chem.*, 1996, **68**, 2155–2163.

4 (*a*) I. Ali, O. M. L. Alharbi and M. M. Sanagi, *Environ. Chem. Lett.*, 2016, **14**, 79–98; (*b*) M. Pumera, *Electrophoresis*, 2006, **27**, 244–256.

5 (*a*) S. Ehlert, A. Walte and R. Zimmermann, *Anal. Chem.*, 2013, **85**, 11047–11053; (*b*) X. Liang, Q. Zhou, W. Wang, X. Wang, W. Chen, C. Chen, Y. Li, K. Hou, J. Li and H. Li, *Anal. Chem.*, 2013, **85**, 4849–4852.

6 (*a*) G. W. Dicinoski, R. A. Shellie and P. R. Haddad, *Anal. Lett.*, 2006, **39**, 639–657; (*b*) G.-H. L. Lang and K. M. J. Boyle, *Forensic Sci.*, 2009, **54**, 1315–1322.

7 M. Bottegal, L. Lang, M. Miller and B. McCord, *Rapid Commun. Mass Spectrom.*, 2010, **24**, 1377–1386.

8 (*a*) J. J. Bellucci, A. Simonetti, C. Wallace, E. C. Koeman and P. C. Burns, *Anal. Chem.*, 2013, **85**, 4195–4198; (*b*) A. P. Packer, D. Lariviere, C. Li, M. Chen, A. Fawcett, K. Nielsen, K. Mattson, A. Chatt, C. Scriver and L. S. Erhardt, *Anal. Chim. Acta*, 2007, **588**, 166–172; (*c*) G. Gillen, C. Szakal and T. M. Brewer, *Surf. Interface Anal.*, 2011, **43**, 376–379; (*d*) M. Luo, B. Hu, X. Zhang, D. Peng, H. Chen, L. Zhang and Y. Huan, *Anal. Chem.*, 2009, **82**, 282–289; (*e*) J. J. Perez, P. M. Flanigan, J. J. Brady and R. J. Levis, *Anal. Chem.*, 2012, **85**, 296–302.

9 (*a*) F. Zapata, M. López-López and C. García-Ruiz, *Appl. Spectrosc. Rev.*, 2016, **51**, 207–242; (*b*) J. Yinon, *Counterterrorist Detection Techniques of Explosives*, Elsevier, 2011, 454; (*c*) J. Yinon and S. Zitrin, *Modern Methods and Applications in Analysis of Explosives*, John Wiley & Sons, 1996, 316; (*d*) M. Marshall and J. C. Oxley, *Aspects of Explosives Detection*, Elsevier, 2011, 302.

10 W. Lu, S. A. Asher, Z. Meng, Z. Yan, M. Xue, L. Qiu and D. Yi, *J. Hazard. Mater.*, 2016, **316**, 87–93.

11 J. Li, C. E. Kendig and E. E. Nesterov, *J. Am. Chem. Soc.*, 2007, **129**, 15911–15918.

12 (*a*) S. Lordel, F. Chapuis-Hugon, V. Eudes and V. Pichon, *J. Chromatogr. A*, 2010, **1217**, 6674–6680; (*b*) Y. Ma, S. Xu, S. Wang and L. Wang, *TrAC, Trends Anal. Chem.*, 2015, **67**, 209–216.

13 For the most recent reviews see: X. Sun, Y. Wang and Y. Lei, *Chem. Soc. Rev.*, 2015, **44**, 8019–8061.

14 (*a*) Y. Geng, M. A. Ali, A. J. Clulow, S. Fan, P. L. Burn, I. R. Gentle, P. Meredith and P. E. Shaw, *Nat. Commun.*, 2015, **6**, 8240; (*b*) L. Guo, B. Zu and X. Dou, *Chem. Sci. J.*, 2014, **5**, 1–2; For reviews see: (*c*) Y. Salinas, R. Martínez-Máñez, M. D. Marcos, F. Sancenón, A. M. Costero, M. Parra and S. Gil, *Chem. Soc. Rev.*, 2012, **41**, 1261–1296; (*d*) G. V. Zyryanov, D. S. Kopchuk, I. S. Kovalev, E. V. Nosova, V. L. Rusinov and O. N. Chupakhin, *Russ. Chem. Rev.*, 2014, **83**, 783–819; (*e*) S. J. Toal and W. C. Trogler, *J. Mater. Chem.*, 2006, **16**, 2871–2883.

15 For FIDO device see: (*a*) C. J. Cumming, C. Aker, M. Fisher, M. Fox, M. J. la Grone, D. Reust, M. G. Rockley, T. M. Swager, E. Towers and V. Williams, *IEEE Trans. Geosci. Remote Sens.*, 2001, **39**, 1119–1128; For ''Nitroscan'' device see: (*b*) E. V. Verbitskiy, A. A. Baranova, K. I. Lugovik, M. Z. Shafikov, K. O. Khokhlov, E. M. Cheprakova, G. L. Rusinov, O. N. Chupakhin and V. N. Charushin, *Anal. Bioanal. Chem.*, 2016, **408**, 4093–4101.

16 J. R. Lakowicz, *Principles of Fluorescence Spectroscopy*, Springer, 3rd edn, 2000, ISBN: 978-0-387-31278-1.

17 (*a*) B. Gole, S. Shanmugaraju, A. K. Bar and P. S. Mukherjee, *Chem. Commun.*, 2011, **47**, 10046–10048; (*b*) B. Gole, W. Song, M. Lackinger and P. S. Mukherjee, *Chem. – Eur. J.*, 2014, **20**, 13662–13680; (*c*) D. T. McQuade, A. E. Pullen and T. M. Swager, *Chem. Rev.*, 2000, **100**, 2537–2574; (*d*) D. Zhao and T. M. Swager, *Macromolecules*, 2005, **38**, 9377–9384; (*e*) Y. Liu, R. C. Mills, J. M. Boncella and K. S. Schanze, *Langmuir*, 2001, **17**, 7452–7455; For polymetaloles see: (*f*) H. Sohn, M. J. Sailor, D. Magde and W. C. Trogler, *J. Am. Chem. Soc.*, 2003, **125**, 3821–3830; (*g*) H. Sohn, R. M. Calhoun, M. J. Sailor and W. C. Trogler, *Angew. Chem.*, 2001, **113**, 2162–2163 (*Angew. Chem., Int. Ed.*, 2001, **40**, 2104–2105); (*h*) J. C. Sanchez, A. G. Di Pasquale, A. L. Rheingold and W. C. Trogler, *Chem. Mater.*, 2007, **19**, 6459–6470; For heteroaromatic polymers see: (*i*) H. Nie, Y. Zhao, M. Zhang, Y. Ma, M. Baumgarten and K. Mullen, *Chem. Commun.*, 2011, **47**, 1234–1236; (*j*) L.-L. Zhou, M. Li, H.-Y. Lu and C.-F. Chen, *Polym. Chem.*, 2016, **7**, 310–318.

18 (*a*) D. A. Olley, E. J. Wren, G. Vamvounis, M. J. Fernee, X. Wang, P. L. Burn, P. Meredith and P. E. Shaw, *Chem. Mater.*, 2011, **23**, 789–794; (*b*) M. Guo, O. Varnavski, A. Narayanan, O. Mongin, J.-P. Majoral, M. Blanchard-Desce and T. Goodson, *J. Phys. Chem. A*, 2009, **113**, 4763–4771; (*c*) G. Tang, S. S. Y. Chen, P. E. Shaw, K. Hegedus, X. Wang, P. L. Burn and P. Meredith, *Polym. Chem.*, 2011, **2**, 2360–2368; (*d*) P. E. Shaw, H. Cavaye, S. S. Y. Chen, M. James, I. R. Gentle and P. L. Burn, *Phys. Chem. Chem. Phys.*, 2013, **15**, 9845–9853; (*e*) Z. Ding, Q. Zhao, R. Xing, X. Wang, J. Ding, L. Wang and Y. Han, *J. Mater. Chem. C*, 2013, **1**, 786–792.

19 (*a*) K. Shiraishi, T. Sanji and M. Tanaka, *ACS Appl. Mater. Interfaces*, 2009, **1**, 1379–1382; (*b*) Y. H. Lee, H. Liu, J. Y. Lee, S. H. Kim, S. K. Kim, J. L. Sessler, Y. Kim and J. S. Kim, *Chem. – Eur. J.*, 2010, **16**, 5895–5901; (*c*) P. D. Barata and J. V. Prata, *Supramol. Chem.*, 2013, **25**, 782–797; (*d*) K. S. Prakash and R. Nagarajan, *Tetrahedron*, 2013, **69**, 8269–8275; (*e*) Z.-F. An, C. Zheng, R.-F. Chen, J. Yin, J.-J. Xiao, H.-F. Shi, Y. Tao, Y. Qian and W. Huang, *Chem. – Eur. J.*, 2012, **18**, 15655–15661; (*f*) X. Qiu, R. Lu, H. Zhou, X. Zhang, T. Xu, X. Liu and Y. Zhao, *Tetrahedron Lett.*, 2007, **48**, 7582–7585; (*g*) E. V. Verbitskiy, A. A. Baranova, K. I. Lugovik, K. O. Khokhlov, E. M. Cheprakova, G. L. Rusinov, O. N. Chupakhin and V. N. Charushin, *ARKIVOC*, 2016, **iii**, 360–373; (*h*) Y. Z. Liao, V. Strong, Y. Wang, X.-G. Li, X. Wang and R. B. Kaner, *Adv. Funct. Mater.*, 2012, **22**, 726–735; (*i*) S. Satapathi, A. Bheemaraju, S. K. Surampudi, D. Venkataraman and J. Kumar, *IEEE Sens. J.*, 2014, **14**, 4334–4339; (*j*) D. S. Kim, V. M. Lynch, K. A. Nielsen, C. Johnsen, J. O. Jeppesen and J. L. Sessler, *Anal. Bioanal. Chem.*, 2009, **395**, 393–400; (*k*) B. M. Rambo and J. L. Sessler, *Chem. – Eur. J.*, 2011, **17**, 4946–4959; (*l*) S. Tao, G. Li and H. Zhu, *J. Mater. Chem.*,

2006, **16**, 4521–4528; (*m*) S. Y. Tao and G. T. Li, *Colloid Polym. Sci.*, 2007, **285**, 721–728; (*n*) M. Li, W. Yuquan and Y. Nan, *Adv. Mater. Res.*, 2013, **652–654**, 1912–1915.

20 (*a*) B. Gole, A. K. Bar and P. S. Mukherjee, *Chem. Commun.*, 2011, **47**, 12137–12139; (*b*) S. Ghosh and P. S. Mukherjee, *Organometallics*, 2008, **27**, 316–319; (*c*) A. Lan, K. Li, H. Wu, D. H. Olson, T. J. Emge, W. Ki, M. Hong and J. Li, *Angew. Chem., Int. Ed.*, 2009, **48**, 2334–2338; For recent reviews see: (*d*) L. E. Kreno, K. Leong, O. K. Farha, M. Allendorf, R. P. Van Duyne and J. T. Hupp, *Chem. Rev.*, 2012, **112**, 1105–1125; (*e*) P. Kumar, A. Deep and K.-H. Kim, *TrAC, Trends Anal. Chem.*, 2015, **73**, 39–53.

21 For pyrene-containing materials see: (*a*) W. Chen, N. B. Zuckerman, J. P. Konopelski and S. Chen, *Anal. Chem.*, 2010, **82**, 461–465; (*b*) S. Burattini, H. M. Colquhoun, B. W. Greenland, W. Hayes and M. Wade, *Macromol. Rapid Commun.*, 2009, **30**, 459–463; (*c*) L. HuiHui, L. FengTing, Z. ShuJuan, H. Gang and F. Yu, *Chin. Sci. Bull.*, 2008, **53**, 1644–1650; (*d*) Y. Wang, A. La, Y. Ding, Y. Liu and Y. Lei, *Adv. Funct. Mater.*, 2012, **22**, 3547–3555; (*e*) G. Lin, H. Ding, D. Yuan, B. Wang and C. Wang, *J. Am. Chem. Soc.*, 2016, **138**, 3302–3305; For pyrene oligomers see: (*f*) H. Bai, C. Li and G. Q. Shi, *Sens. Actuators, B*, 2008, **130**, 777–782; (*g*) Y. Chen, H. Bai, Q. Chen, C. Li and G. Shi, *Sens. Actuators, B*, 2009, **138**, 563–571; For single-molecule pyrene-based sensors see: (*h*) A. D. Hughes, I. C. Glenn, A. D. Patrick, A. Ellington and E. V. Anslyn, *Chem. – Eur. J.*, 2008, **14**, 1822–1827; (*i*) J. V. Goodpaster and V. L. McGuffin, *Anal. Chem.*, 2001, **73**, 2004–2011; (*j*) S. Shanmugaraju, S. A. Joshi and P. S. Mukherjee, *J. Mater. Chem.*, 2011, **21**, 9130–9138; (*k*) J.-H. Hong, J.-H. Choi and D.-G. Cho, *Bull. Korean Chem. Soc.*, 2014, **35**, 3158–3162; (*l*) I. S. Kovalev, O. S. Taniya, N. V. Slovesnova, G. A. Kim, S. Santra, G. V. Zyryanov, D. S. Kopchuk, A. Majee, V. N. Charushin and O. N. Chupakhin, *Chem. – Asian J.*, 2016, **11**, 775–781; (*m*) S. K. Kim, J. M. Lim, T. Pradhan, H. S. Jung, V. M. Lynch, J. S. Kim, D. Kim and J. L. Sessler, *J. Am. Chem. Soc.*, 2014, **136**, 495–505.

22 R. V. Taudte, A. Beavis, L. Wilson-Wilde, C. Roux, P. Doble and L. Blanes, *Lab Chip*, 2013, **13**, 4164–4172.

23 (*a*) J.-S. Yang and T. M. Swager, *J. Am. Chem. Soc.*, 1998, **120**, 5321–5322; (*b*) J.-S. Yang and T. M. Swager, *J. Am. Chem. Soc.*, 1998, **120**, 11864–11873.

24 (*a*) T. M. Swager, *Acc. Chem. Res.*, 1998, 201–207; (*b*) S. W. Thomas, G. D. Joly and T. M. Swager, *Chem. Rev.*, 2007, **107**, 1339–1386.

25 For reviews see: (*a*) J. H. Chong and M. J. MacLachlan, *Chem. Soc. Rev.*, 2009, **38**, 3301–3315; (*b*) J. Cao, Y. Jiang and C. Chen, *Prog. Chem.*, 2011, **23**, 2200–2214; (*c*) Y. Jiang and C.-F. Chen, *Eur. J. Org. Chem.*, 2011, 6377–6403; (*d*) J. Cao, Y. Jiang and C.-F. Chen, *Prog. Chem.*, 2011, **23**, 2200–2214; (*e*) S. Rochat and T. M. Swager, *ACS Appl. Mater. Interfaces*, 2013, **5**, 4488–4502; (*f*) Y.-X. Ma, Z. Meng and C.-F. Chen, *Synlett*, 2015, 6–30.

26 M. A. Enlow, *J. Mol. Graphics Modell.*, 2012, **33**, 12–18.

27 (*a*) P. Anzenbacher, Jr., L. Mosca, M. A. Palacios, G. V. Zyryanov and P. Koutnik, *Chem. – Eur. J.*, 2012, **18**, 12712–12718; (*b*) L. Mosca, P. Koutník, V. M. Lynch, G. V. Zyryanov, N. A. Esipenko and P. Anzenbacher, *Cryst. Growth Des.*, 2012, **12**, 6104–6109.

28 G. V. Zyryanov, M. A. Palacios and P. Anzenbacher Jr., *Org. Lett.*, 2008, **10**, 3681–3684.

29 For turn-off fluorescence chemosensors/probes/materials for the detection of nitrate esters and nitramines (including RDX), see: (*a*) A. Ponnu and E. V. Anslyn, *Supramol. Chem.*, 2010, **22**, 65–71; (*b*) D. Gopalakrishnan and W. R. Dichtel, *J. Am. Chem. Soc.*, 2013, **135**, 8357–8362; (*c*) J. C. Sanchez and W. C. Trogler, *J. Mater. Chem.*, 2008, **18**, 3143–3156; (*d*) R. Freeman and I. Willner, *Nano Lett.*, 2009, 1322–1326; (*e*) C. Wang, H. Huang, B. R. Bunes, N. Wu, M. Xu, X. Yang, L. Yu and L. Zang, *Sci. Rep.*, 2016, **6**, 25015; For turn-on approaches see: (*f*) T. L. Andrew and T. M. Swager, *J. Am. Chem. Soc.*, 2007, **129**, 7254–7255; (*g*) L. Mosca, S. K. Behzad and P. Anzenbacher, Jr., *J. Am. Chem. Soc.*, 2015, **137**, 7967–7969.

30 G. Venkataramana and S. Sankararaman, *Eur. J. Org. Chem.*, 2005, 4162–4166.

31 Cambridge Crystallographic Data Centre Number is CCDC 1486665.

32 Q. Zhou and T. M. Swager, *J. Am. Chem. Soc.*, 1995, **117**, 12593–12602.

33 Cambridge Crystallographic Data Centre Number is CCDC 1485942.

34 For the pyrene complexes with aromatic compounds see: (*a*) H. Sun, M. Wang, X. Wei, R. Zhang, S. Wang, A. Khan, R. Usman, Q. Feng, M. Du, F. Yu, W. Zhang and C. Xu, *Cryst. Growth Des.*, 2015, **15**, 4032–4038; For pyrene complexes with nitroaromatic compounds see: (*b*) J. C. Barnes, J. A. Chudeck, R. Fosma, F. Jarrett, F. Mackie, J. Paton and D. R. Twiselton, *Tetrahedron*, 1984, **40**, 1595–1601; (*c*) J. C. Barnes and W. Golnazarians, *Acta Crystallogr., Sect. A: Found. Crystallogr.*, 1987, **C43**, 549–552; (*d*) C. K. Prout and I. J. Tickle, *J. Chem. Soc., Perkin Trans. 2*, 1973, 734–737.

35 N. J. Turro, V. Ramamurthy and J. C. Scaiano, *Principles of Molecular Photochemistry*, Academic press, Sausalito, 2009.

36 G. Gauglitz and T. Vo-Dinh, *Handbook of Spectroscopy*, John Wiley & Sons, 2006, 1168.

37 B. Valeur, *Molecular Fluorescence. Principles and Applications*, Wiley-VCH, Weinheim, 2002.

38 (*a*) H. Fang, F. Mighri and A. Ajji, *Polym. Eng. Sci.*, 2007, **47**, 192–199; (*b*) J. Yan and M. A. Winnik, *Can. J. Chem.*, 1995, **73**, 1823–1830.

39 M. J. Frisch, G. W. Trucks, H. B. Schlegel, G. E. Scuseria, M. A. Robb, J. R. Cheeseman, G. Scalmani, V. Barone, B. Mennucci, G. A. Petersson, H. Nakatsuji, M. Caricato, X. Li, H. P. Hratchian, A. F. Izmaylov, J. Bloino, G. Zheng, J. L. Sonnenberg, M. Hada, M. Ehara, K. Toyota, R. Fukuda, J. Hasegawa, M. Ishida, T. Nakajima, Y. Honda, O. Kitao, H. Nakai, T. Vreven, J. A. Montgomery Jr., J. E. Peralta, F. Ogliaro, M. Bearpark, J. J. Heyd, E. Brothers, K. N. Kudin, V. N. Staroverov, R. Kobayashi, J. Normand, K. Raghavachari, A. Rendell, J. C. Burant, S. S. Iyengar, J. Tomasi, M. Cossi, N. Rega, J. M. Millam, M. Klene, J. E. Knox, J. B. Cross, V. Bakken, C. Adamo, J. Jaramillo, R. Gomperts, R. E. Stratmann,

O. Yazyev, A. J. Austin, R. Cammi, C. Pomelli, J. W. Ochterski, R. L. Martin, K. Morokuma, V. G. Zakrzewski, G. A. Voth, P. Salvador, J. J. Dannenberg, S. Dapprich, A. D. Daniels, Ö. Farkas, J. B. Foresman, J. V. Ortiz, J. Cioslowski and D. J. Fox, *Gaussian 09, Revision D.01*, Gaussian, Inc., Wallingford CT, 2009.

40 A. Austin, G. Petersson, M. J. Frisch, F. J. Dobek, G. Scalmani and K. Throssell, *J. Chem. Theory Comput.*, 2012, **8**, 4989–5007.

41 F. Weigend and R. Ahlrichs, *Phys. Chem. Chem. Phys.*, 2005, **7**, 3297–3305.

42 L. A. Estrada, V. A. Montes, G. Zyryanov and P. Anzenbacher Jr., *J. Phys. Chem. B*, 2007, **111**, 6983–6986.

43 (*a*) B. C. Dionne, D. P. Rounbehler, E. K. Achter, J. R. Hobbs and D. H. Fine, *J. Energ. Mater.*, 1986, **4**, 447–472; (*b*) *Vapor Pressures at 25 °C, Handbook of Physical Properties of Organic-Chemicals*, ed. D. R. Lide, CRC, Boca Raton, FL, 1997.

